Antiferromagnetic Porous Metal-Organic Framework Containing Mixed-Valence [(Mn4Mn2III)-Mn-II (mu(4)-O)(2)](10+) Units with Catecholase Activity and Selective Gas Adsorption

ARTICLE *in* INORGANIC CHEMISTRY · MARCH 2012

Impact Factor: 4.76 · DOI: 10.1021/ic2027362 · Source: PubMed

4 AUTHORS:

Paramita Kar
Hokkaido University
15 PUBLICATIONS **286** CITATIONS
SEE PROFILE

Ritesh Haldar
Jawaharlal Nehru Centre for Advanced Scienti…
27 PUBLICATIONS **359** CITATIONS
SEE PROFILE

Carlos J Gómez-García
University of Valencia
362 PUBLICATIONS **9,455** CITATIONS
SEE PROFILE

Ashutosh Ghosh
University of Calcutta
211 PUBLICATIONS **3,832** CITATIONS
SEE PROFILE

Inorganic Chemistry

Article

pubs.acs.org/IC

Antiferromagnetic Porous Metal–Organic Framework Containing Mixed-Valence $[Mn^{II}_4Mn^{III}_2(\mu_4\text{-}O)_2]^{10+}$ Units with Catecholase Activity and Selective Gas Adsorption

Paramita Kar,[†] Ritesh Haldar,[‡] Carlos J. Gómez-García,*[,§] and Ashutosh Ghosh*[,†]

[†]Department of Chemistry, University College of Science, University of Calcutta, 92, APC Road, Kolkata-700 009, India

[‡]New Chemistry Unit, Jawaharlal Nehru Centre for Advanced Scientific Research, Jakkur, Bangalore 560064, India

[§]Instituto de Ciencia Molecular (ICMol), C/Catedrático José Beltrán 2, Parque Científico, Universidad de Valencia, 46980 Paterna, Valencia, Spain

Supporting Information

ABSTRACT: A multifunctional porous metal organic framework based on mixed-valence hexa-nuclear $[Mn^{III}_2Mn^{II}_4O_2(pyz)_2(C_6H_5CH_2COO)_{10}]$ (pyz = pyrazine) units has been synthesized. The complex has been characterized by elemental analysis, IR spectroscopy, single-crystal X-ray diffraction analysis, and variable-temperature magnetic measurements. The structural analysis reveals that the bidentate pyz molecules connect each $[Mn_6]$ unit to its four $[Mn_6]$ neighbors through the peripheral Mn(II) centers, giving rise to a three-dimensional (3D) distorted diamond-like porous framework. Variable-temperature (2–300 K) magnetic susceptibility measurements show the presence of dominant antiferromagnetic interactions within the discrete $[Mn_6]$ cluster that have been fitted with a model containing three exchange constants developed for the complex ($J_1 = -8.6$ cm^{-1}, $J_2 = -3.9$ cm^{-1}, and $J_3 = -100.0$ cm^{-1}). Using 3,5-di-*tert*-butyl catechol (3,5-DTBC) as the substrate, catecholase activity of the complex has been studied; the turn over number is determined to be of 2547 h^{-1} in acetonitrile. This porous compound shows remarkable selectivity for adsorption of CO_2 over N_2 that may be correlated with the effect of window flexibility of the pore to the corresponding adsorbate molecules.

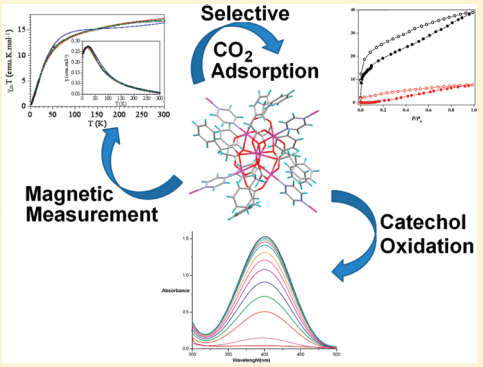

INTRODUCTION

Current interest in the development of multifunctional materials is rapidly expanding because of their intriguing properties and their potential applications in various fields, for example, catalysis, adsorption, storage, magnetism, molecular recognition, fluorescence, nonlinear optics, and sensors.[1] The molecular materials which are synthesized aiming primarily to study one property can be made multifunctional by judicious choice of metal ions and ligands. For example, by connecting polynuclear metal clusters with suitable linkers, it is possible to prepare materials showing gas adsorption, fluorescence, or catalytic activity besides magnetism.[2] The construction of magnetic metal–organic frameworks (MOFs) based on metallic cluster building blocks is still a major challenge mainly because of two interrelated aspects: (i) it is difficult to find appropriate polymeric magnetic building blocks able to act as node and stable enough to resist decomposition during the polymerization reaction, and (ii) the linkers between the building blocks should be capable of retaining and/or transmitting the inherent properties of the metallic cluster to the extended system and should also be inactive enough to avoid the decomposition of the metallic cluster core into monomeric complexes.[3]

Manganese-based coordination compounds have received considerable attention in recent years not only for their remarkable magnetic properties that have led to the development of a new class of compounds called single-molecule magnets (SMMs),[4] but also for their rich biochemistry[5] and catalytic activity.[6] In this regard, the hexanuclear carboxylate clusters of the type $[Mn_6O_2(RCO_2)_{10}L_4]$ deserve special mention for their magnetic properties at very low temperatures that has given rise to a specific family of single-molecule magnets (SMMs).[7] More recently, attention has been paid to the use of this type of clusters as tectonic fragments for the synthesis of polymeric materials, since these clusters may introduce their inherent physical properties into the polymeric networks.[8] The extraordinary stability of the mixed valence $[Mn_6O_2]$ core makes them very promising as building blocks for the preparation of such polymeric materials.

Our study has focused on the possibility of networking this class of particularly stable $[Mn_6]$ coordination clusters, that is, hexanuclear manganese carboxylate clusters of formula $[Mn_6O_2(O_2CR)_{10}L_4]$ (L = neutral monodentate ligand), in which L can be completely or partially replaced by different

Received: December 21, 2011
Published: March 14, 2012

   dx.doi.org/10.1021/ic2027362 | *Inorg. Chem.* 2012, 51, 4265–4273

bridging ligands to construct polymeric frameworks based on the $[Mn_6]$ core with a connectivity up to four where the $[Mn_6]$ cluster remains intact. Although the structure of the $[Mn_6O_2(RCOO)_{10}]$ cluster is quite common,[9] very few of them are further linked to produce polymeric structures. Replacement of the neutral capping ligand, L, by an exobidentate linker mainly produces one-dimensional (1D) structures (both linear and zigzag chains),[8,10] although one dumbbell shaped dimer[10] and one three-dimensional (3D) hexagonal-like motif[10] have also been reported.

Herein, we report the synthesis, X-ray single crystal structure analysis and variable temperature magnetic study of a $[Mn_6]$ based unique 3D diamond-like porous complex $[Mn^{III}_2Mn^{II}_4O_2(pyz)_2(C_6H_5CH_2COO)_{10}]_n$, where pyz = pyrazine. The compound also exhibits appreciably high catecholase activity. Although, manganese coordination compounds are a potential source of homogeneous catalysts (because of their low cost and toxicity),[11] it is quite surprising that catalytic activity of $[Mn_6]$ based clusters are still not investigated. Moreover, short and rigid pyz linker and bulky, flexible phenyl acetate anion create a 3D porous framework that introduces molecular sieving properties to the compound as demonstrated by its selective CO_2 adsorption. To the best of our knowledge, this is the first time that these properties (catalytic activity and selective gas adsorption) are observed in a MOF based on a magnetic cluster.

EXPERIMENTAL SECTION

Starting Materials. The metal carboxylate salt, that is, $Mn(C_6H_5CH_2COO)_2{\cdot}H_2O$ was synthesized by adding manganese carbonate (60 mg) to a solution of phenyl acetic acid (136.15 mg) in 30 mL of water with constant stirring with a glass-rod until effervescence was stopped. Then the solution was filtered, and the clear filtrate was kept over a water bath until a solid started to separate. The solution was then cooled to room temperature, and the solid was filtered through suction and dried in vacuum. All other chemicals are commercial and were of reagent grade and used as received, without further purification.

Synthesis of $[Mn^{III}_2Mn^{II}_4O_2(pyz)_2(C_6H_5CH_2COO)_{10}]_n$. An ethanolic (10 mL) solution of pyz (0.160 g, 2 mmol) was added to a solution of $Mn(C_6H_5CH_2COO)_2{\cdot}H_2O$ (0.343 g, 1 mmol) in 5 mL of ethanol. The resulting mixture was put under reflux for about 2 h, cooled, and filtered. The resulting clear filtrate gave a pale yellow solid after standing for 1−2 days at room temperature. The yellow solid was dissolved in CH_3CN and filtered. The colorless filtrate gradually turned to brown, and brown plate-like single-crystals suitable for X-ray diffraction were obtained by slow evaporation of the mother liquor after several days.

Complex **1**: Yield: 0.227 g; 73%. Anal. Calcd. for $C_{88}H_{78}Mn_6N_4O_{22}$ (1873.18): C, 56.42; H, 4.20; N, 2.99 Found: C, 56.40; H, 4.17; N, 2.97. IR (KBr pellet, cm^{-1}): 1599 ν_{as}(COO), 1395 ν_s(COO).

Physical Measurements. Elemental analyses (carbon, hydrogen, and nitrogen) were performed using a Perkin-Elmer 240C elemental analyzer. IR spectra in KBr (4500−500 cm^{-1}) were recorded using a Perkin-Elmer RXI FT-IR spectrophotometer. The electronic absorption spectra (1000−200 nm) of the complex were recorded in CH_3CN with a Hitachi U-3501 spectrophotometer. Magnetic susceptibility measurements were carried out in the temperature range 2−300 K with an applied magnetic field of 0.1 T on a polycrystalline sample of compound **1** (mass = 39.24 mg) with a Quantum Design MPMS-XL-5 SQUID susceptometer. The isothermal magnetization was performed on the same sample at 2 K with magnetic fields up to 5 T. The susceptibility data were corrected for the sample holders previously measured using the same conditions and for the diamagnetic contributions of the salt as deduced by using Pascals' constant tables (χ_{dia} = −876.54 × 10^{-6} emu.mol^{-1}).[12] The adsorption isotherm of CO_2 (195 K) and N_2 (77 K) were measured by using a Quantachrome Quadrasorb-*SI* adsorption instrument. In the sample chamber (~17.5 mL) maintained at $T \pm 0.03$ K was placed the adsorbent sample (~100−150 mg), prepared at 373 K under a 10^{-1} Pa vacuum for about 12 h prior to measurement of the isotherms. Helium gas at a certain pressure was introduced in the gas chamber and allowed to diffuse into the sample chamber by opening the valve. The change in pressure allowed an accurate determination of the volume of the total gas phase. The amount of gas adsorbed was calculated readily from pressure difference ($P_{cal} - P_e$), where P_{cal} is the calculated pressure with no guest adsorption and P_e is the observed equilibrium pressure. All operations were computer-controlled and automatic.

Crystallographic Data Collection and Refinement. A single crystal of the complex was mounted on a Bruker SMART diffractometer equipped with a graphite monochromator and Mo−Kα (λ = 0.71073 Å) radiation. The crystal was positioned at 60 mm from the CCD. 360 frames were measured with a counting time of 10 s. The structures were solved using the Patterson method by using the SHELXS97. Subsequent difference Fourier synthesis and least-squares refinement revealed the positions of the remaining non hydrogen atoms. Non-hydrogen atoms were refined with independent anisotropic displacement parameters. Hydrogen atoms were placed in idealized positions, and their displacement parameters were fixed to be 1.2 times larger than those of the attached non-hydrogen atom. Successful convergence was indicated by the maximum shift/error of 0.001 for the last cycle of the least-squares refinement. In the complex, two $CH_2-C_6H_5$ rings with unreasonable thermal parameters were refined as disordered each with two sets of sites. Atoms in these sets were refined isotropically with population parameters refining to 0.52(2), 0.57(1), respectively. Absorption corrections were carried out using the SADABS program.[13] All calculations were carried out using SHELXS 97,[14] SHELXL 97,[15] PLATON 99,[16] ORTEP-32,[17] and WinGX systemVer-1.64.[18] Data collection and structure refinement parameters and crystallographic data for the complex are given in the Supporting Information, Table ST1.

RESULTS AND DISCUSSION

Synthesis. The reaction between $Mn(C_6H_5CH_2COO)_2{\cdot}H_2O$ and pyz in C_2H_5OH gave a yellow amorphous complex $[Mn^{II}(pyz)(C_6H_5CH_2COO)_2]$ as confirmed by elemental analysis. This compound was dissolved in acetonitrile and stirred for about 2 h, resulting in a color change from pale yellow to brown. On keeping the solution at ambient conditions for several days, brown single crystals of compound **1** started to separate (Scheme 1). These crystals were crystallographically identified as a mixed-valence 3D polymer containing four Mn(II) and two Mn(III) ions in the basic hexanuclear unit. The starting manganese source contains only Mn(II) ions and thus it is clear that the Mn(III) ions are formed by aerial oxidation, as indicated by the color change

Scheme 1. Formation of the Complex 1

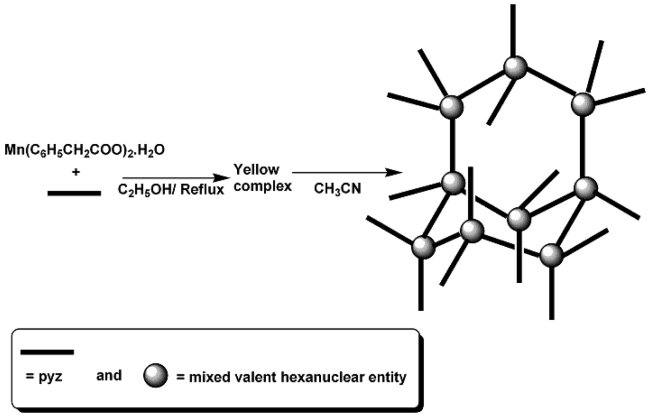

dx.doi.org/10.1021/ic2027362 | Inorg. Chem. 2012, 51, 4265−4273

from pale yellow to brown during stirring. The solvent plays a prominent role in the synthesis of the compound. To get compound **1**, the yellow compound must be dissolved in acetonitrile; if the same process is carried out in ethanol, in methanol, or in dichloromethane, the starting amorphous yellow compound precipitates again. In fact, for the preparation of complexes with the $[Mn^{II}_4Mn^{III}_2O_2]^{10+}$ core by aerial oxidation, acetonitrile is the most commonly used solvent,[9c,19a] although pyridine, dichloromethane, and ethanol have also been used in some cases.[19b−d]

Description of Structure of Complex 1. The single-crystal X-ray structural analysis shows that complex **1** crystallizes in the monoclinic space group *C*2/*c* with the $[Mn_6]$ core located on a 2-fold axis, which passes through Mn1 and Mn2 along the crystallographic *b* axis, and hence the asymmetric unit contains only half of the cluster. A view of the structure of the $[Mn_6]$ cluster with the atom labeling scheme is shown in Figures 1 and 2. Selected bond lengths and angles of complex **1** are summarized in the Supporting Information, Table ST2.

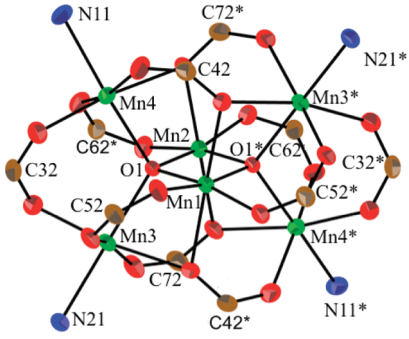

Figure 1. Central $[Mn_6]$ cluster in complex **1** with ellipsoids at 50% probability (symmetry code * = −*x*, *y*, 1/2 − *z*). All hydrogen atoms and phenyl rings have been omitted for clarity.

The central core contains six manganese centers with an octahedral environment, two Mn(III) (Mn1 and Mn2) and four Mn(II) ions (Mn3, Mn4, Mn3*, and Mn4*,where * = −*x*, *y*, 1/2 − *z*). The metal atoms are located in the vertex of two Mn^{II}_2-Mn^{III}_2 tetrahedra sharing their Mn(III)−Mn(III) edge with a μ_4 oxygen atom (O1) in the center of each tetrahedron, giving rise to a $[Mn^{III}_2M^{II}_4O_2]$ unit (Figure 2a).

The octahedral coordination of each Mn(II) ion is of the type MnO_5N, with four O atoms from four carboxylate groups, one O from the central μ_4-O1 bridge, and a N from a pyz (connecting each $[Mn_6]$ cluster with its four neighbors). The two central Mn(III) ions (Mn1 and Mn2) present elongated octahedral environments. In Mn1 the equatorial plane involves two μ-O atoms, O51 and O51* at 1.956(5) Å and two μ_4-O atoms, O1 and O1* at 1.886(4) Å. The axial positions are occupied by two μ-O atoms O41 and O41* from two symmetry-related μ_3-bridging carboxylate ligands with a bond length of 2.286(3) Å. In Mn2 the equatorial plane is formed by two μ-O atoms, O61 and O61*, at 1.968(5) Å and two μ_4-O atoms, O1 and O1*, at 1.902(4) Å. As observed in Mn1, the axial positions in Mn2 are occupied by two μ-O atoms, O71 and O71*, from two μ_3-O bridging phenylacetate ligands at 2.227(4) Å. The axial bonds are significantly longer than the equatorial bonds as expected for Jahn−Teller distortion of Mn ions in +3 oxidation state. The Mn1−Mn2 distance is equal to 2.819(2) Å. The bond angles and lengths are very close to those of other reported similar complexes.[19a,19e,20] The average bond lengths around Mn1 (2.042 Å) and Mn2 (2.032 Å) clearly indicate that the oxidation state of these two ions is higher than the oxidation state of Mn3 and Mn4, where the average bond lengths are significantly longer: 2.213 Å and 2.193 Å, respectively. Since the total anionic charge per $[Mn_6]$ cluster is −10, the only possible charge distribution, in agreement with the bond lengths, implies that Mn1 and Mn2 are Mn(III) whereas Mn3 and Mn4 are Mn(II), giving a total charge of +10 (there are two Mn3, two Mn4, one Mn1 and one Mn2 per $[Mn_6]$ cluster).

There are five independent carboxylate groups (centered at C32, C42, C52, C62, and C72). These carboxylates connect all the Mn ions acting as *syn-syn* and also as *syn-anti* κ*O*:κ*O*′. Thus the C32-carboxylate bridges Mn3−Mn4 in a *syn-syn* fashion, C42-carboxylate connects Mn1−Mn4 in a *syn-syn* mode and Mn3−Mn4 in *syn-anti*, C52-carboxylate connects Mn1−Mn3 in *syn-syn*, C62-carboxylate connects Mn2−Mn4 in *syn-syn* and finally, C72-carboxylate bridges Mn1−Mn3 in *syn-syn* and Mn3−Mn4 in *syn-anti* (Figure 1).

The pyz molecules act as κ*N*:κ*N*′ bridging ligands connecting each $[Mn_6]$ cluster with its four neighbors through the peripheral Mn(II) ions. Thus, each pyz bridge connects two Mn4 atoms of neighboring clusters along the *c* axis or two Mn3 atoms (also of neighboring clusters) along the *a* axis, creating a 3D distorted porous diamond-like framework that can be described as a (6,4) net (Figure 3). The complex has potential guest accessible void volume of 81.7 Å^3 (1.0%) per unit cell volume.

Early preparations of diamond-like nets were usually made with metal ions that adopt a strictly tetrahedral geometry.[21]

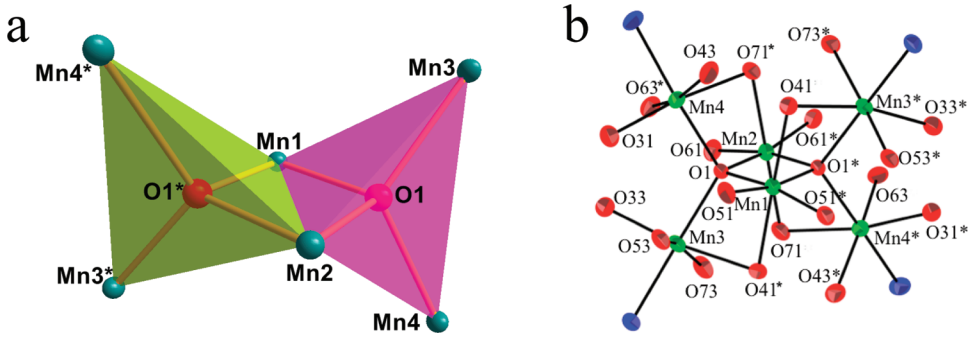

Figure 2. (a) Central $[Mn_6O_2]$ core showing the two edge-sharing tetrahedra with O1 in the center. (b) The coordination environment of the six Mn ions in the central $[Mn_6]$ core.

dx.doi.org/10.1021/ic2027362 | *Inorg. Chem.* 2012, 51, 4265−4273

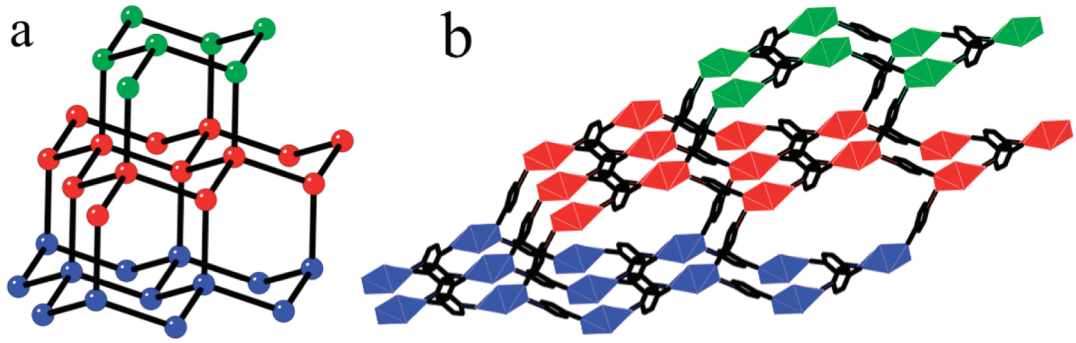

Figure 3. (a) View of the diamond structure and (b) view of an equivalent fragment in the distorted diamond-like topology in compound **1** (C atoms are now replaced by $[Mn_6O_2]$ clusters and the C−C bonds by pyz linkers). Hydrogen atoms and phenylacetate groups have been omitted for clarity.

More recent work has been exploring two other possibilities: (1) the use of metal clusters that take an overall tetrahedral geometry[22] and (2) the use of metal ions with higher coordination numbers that, by blocking some positions, may adopt a pseudotetrahedral coordination geometry, allowing them to act as four-connectors,[23] in a similar manner to that displayed by **1** (Figure 3). In a regular tetrahedron, all the tetrahedral angles are 109.47°, but in this framework the angles between the pyz linkers [117.40(19)° and 74.12(16)°] deviate significantly from the regular tetrahedron.

Compound **1** does not present important π-stacking interactions between the aromatic rings. However, the complex is further stabilized by one C−H···π(phenyl) interaction between the neighboring $[Mn_6]$ cores as shown in Supporting Information, Figure S2. The distance between H67 and the centroid of the phenyl ring of an adjacent core is 2.81 Å and the C67−H67···Cg angle is 142° (Cg = centroid of the phenyl ring).

As we mentioned earlier, although the $[Mn_6O_2(RCOO)_{10}]$ cluster is quite common, polymeric frameworks based on $[Mn_6]$ cores are relatively scarce. In fact, only eight such species have been reported so far.[8,10] Three of them are formed by the complex $[Mn_6O_2Piv_{10}(Thf)_4]$ (Piv = trimethylacetate anion and Thf = tetrahydrofuran) with the linker 2,4,4,5,5-pentamethyl-4,5-dihydro-1*H*-imidazolyl-3-oxide-1-oxyl that yield three different cluster-based coordination polymers when the Thf solvent molecules are partially or completely replaced by the linker, depending on the solvent used in the reaction. Thus, in ethyl acetate the cluster generates nanosized dumbbell-like molecules; in CH_2Cl_2 it forms a 1D chain polymer and in heptane or CCl_4 a 3D hexagonal motif is obtained.[10a] Other three examples were prepared by Kögerler et al. who used pyrazine, nicotinamide, or 1,2-bis(4-pyridyl)-ethane linkers to bridge $[Mn_6O_2(O_2CR)_{10}]$ units in 1D coordination polymers and explored the effect of the flexibility of the spacer on the resulting molecular architechture.[10b] The seventh compound was prepared by Chen et al. with a hexanuclear, mixed-valence $[Mn_6O_2(O_2CEt)_{10}(H_2O)_4]$ cluster which after solvothermal treatment self-assembled with propionato bridges to give a zigzag-like 1D chain polymer.[8b] Finally, Yamashita et al. synthesized a zigzag 1D polymeric chain of molecular formula $[Mn_6O_2(t\text{-}BuCO_2)_{10}(t\text{-}BuCO_2H)_2(bpy)]$ from $[Mn_6O_2(t\text{-}BuCO_2)_{10}(t\text{-}BuCO_2H)_4]$ by replacing the t-$BuCO_2H$ group with 4,4′-bipyridine.[8a] In the present work, we present a pyrazine bridged 3D coordination polymer, $[Mn^{III}_2Mn^{II}_4O_2(pyz)_2(C_6H_5CH_2COO)_{10}]_n$, that has a microporous diamond-like topology that has never been observed in this class of MOFs.

Catecholase Activity Study and Kinetics. Catechol oxidase catalyzes exclusively the oxidation of catechols (i.e., *o*-diphenols) to the corresponding quinones, and this process is known as catecholase activity (Scheme 2) and for this ability

Scheme 2. Catecholase Activity

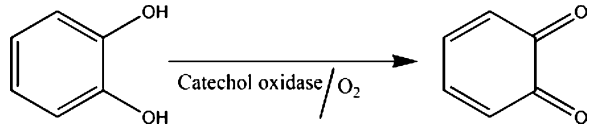

catechol oxidase may take a key role as disease resistant in higher plants. Quinones are highly reactive compounds which undergo auto polymerization to produce melanin, a brown colored pigment, and this process is most likely responsible for protecting damaged tissues against pathogens and insects.

In most of the catecholase activity studies of model complexes 3,5-di-*tert*-butylcatechol (3,5-DTBC) has been chosen as the substrate. Its low redox potential makes it easy to oxidize, and the bulky substituents prevent further reactions such as ring-opening.[24] The oxidation product 3,5-di-*tert*-butylquinone (3,5-DTBQ) is very much stable and exhibits a maximum absorption at 403 nm in pure acetonitrile. Prior to a detailed kinetic study, it is necessary to check the ability of the complex to oxidize 3,5-DTBC. For this purpose, (1.66×10^{-6}) M solution of complex **1** was treated with 100 equiv of 3,5-DTBC under aerobic condition in acetonitrile solution because of the good solubility of the complex, the substrate, and the final product in this solvent. After addition of 3,5-DTBC, the increase of the absorption at ~400 nm, which is indicative of an oxidation from 3,5-DTBC to the corresponding quinone (3,5-DTBQ), indicates a considerable catecholase activity (Figure 4).

We may rationalize our observation in the following way. The oxidation of 3,5-DTBC to 3,5-DTBQ catalyzed by the complex, proceeds via the formation of a catalyst-substrate (CS) adduct whose λ_{max} is close to that of the complex itself. After a few minutes the adduct slowly converts to the quinone[25] as observed in Figure 4. A control experiment has been carried out using manganese(II) phenylacetate instead of complex **1** under analogous conditions to study the possible catalytic activity of a simple Mn salt in the oxidation of 3,5-DTBC to 3,5-DTBQ. Within 1 h of reaction no appreciable amounts of 3,5-DTBQ were noticed by UV−vis spectroscopy.

dx.doi.org/10.1021/ic2027362 | *Inorg. Chem.* 2012, 51, 4265−4273

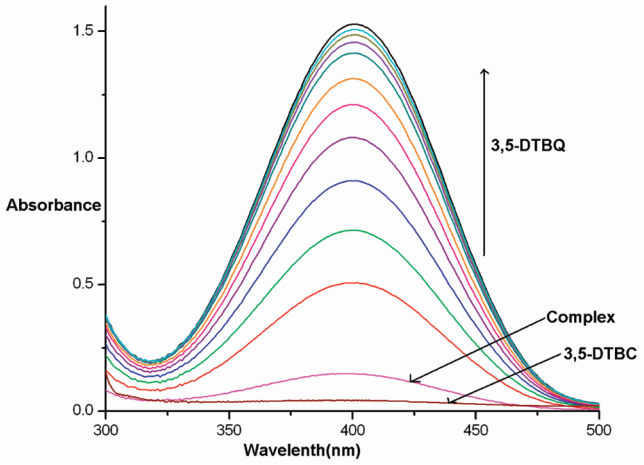

Figure 4. Increase of absorption spectra after addition of 100 equiv of 3,5-DTBC to a solution containing complex **1** (1.66×10^{-6} M) in acetonitrile. The spectra were recorded after every 5 min up to 1 h in CH_3CN.

Kinetic Study. The kinetic study of the oxidation of 3,5-DTBC to 3,5-DTBQ by complex **1** was carried out by monitoring the growth of the absorbance at 400 nm by the initial rates method. To determine the dependence of the rates on the substrate concentration and various kinetic parameters, solutions of complex **1** were prepared with increasing concentrations of 3,5-DTBC (from 10 to 100 equiv) under aerobic conditions at a complex concentration of (1.66×10^{-6}) M. A first-order dependence was observed at low concentrations of the substrate, whereas saturation kinetics was found at higher concentrations of the substrate, as shown in Figure 5.

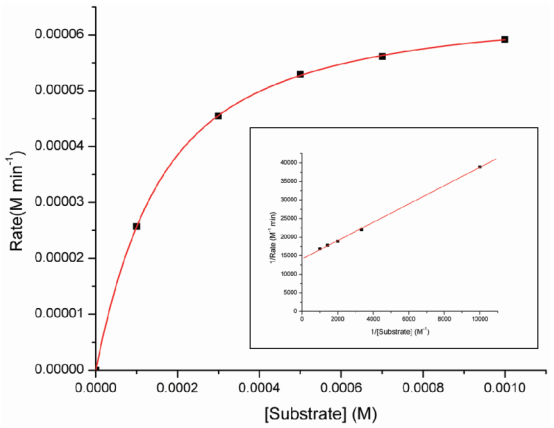

Figure 5. Plot of initial rates vs substrate concentration for the oxidation reaction catalyzed by complex **1**. Inset shows the Lineweaver–Burk plot.

The dependence on the substrate concentration indicates that a catalyst-substrate binding is the initial step in the catalytic mechanism. A treatment on the basis of Michaelis–Menten approach, originally developed for enzyme kinetics, was therefore applied and linearized by means of Lineweaver–Burk plot (double reciprocal) to calculate various kinetic parameters such as Michaelis–Menten constant ($K_M = 1.745 \times 10^{-4}$ (Std. error = 3.213×10^{-5}) M for complex **1**) and maximum initial rate ($V_{max} = 7.076 \times 10^{-5}$ (Std. error 2.703×10^{-6}) M min^{-1} for complex **1**).[25] The turnover number of the complex ($k_{cat} = 2.547 \times 10^3$ h^{-1}) is calculated by dividing the V_{max} value by the complex concentration.

The oxidation process of 3,5-DTBC to 3,5-DTBQ involves two electrons. Literature survey reveals that higher valent metal centers (e.g., Cu^{II}, Mn^{III} and Mn^{IV})[26,27] are usually involved in catechol oxidation; the reports on catecholase activities of manganese(II) complexes are relatively rare.[28] The manganese centers are in +2 and +3 oxidation states in the present complex. Therefore, it is reasonable to consider that in the catalytic cycle Mn(III) undergoes reduction to Mn(II) with concomitant oxidation of 3,5-DTBC to 3,5-DTBQ in the presence of molecular oxygen. Turnover number of the complex (2547 h^{-1}) is higher than those of Krebs et al. and Rajak et al.[29,30] and comparable to those reported by Vittal et al.[31] and Das et al.[25,28a]

Selective CO_2 Adsorption. Since the invention of synthetic-zeolites in the 1940s, with the appearance of various adsorbents and the progress of adsorption-based separation techniques, adsorption has become a key gas separation device in industry.[32] Presence of magnetic property and porosity is not a common phenomena in MOFs as magnetic interactions are good within short-range while porosity requires long linkers. But use of $[Mn_6]$ core based node allows the short-range interactions, and connecting these nodes by some other linkers can also generate porosity. MOFs are attractive because of their modular nature of porosity and are also very useful for selective gas adsorption. This can be attained by using short bridging ligands and increasing the bulkiness of the ligands which constrict the apertures of porous MOFs. In complex **1** the metal coordinated bulky ligand, phenylacetate, and the short bridging ligand pyz satisfy these criteria. To examine the influence of size and polarity of the different adsorbates, we have studied the adsorption properties of the framework of compound **1** with different gases (N_2 and CO_2). The sorption isotherm of N_2 shows no uptake for N_2 (kinetic diameter, 3.64 Å)[33] at 77 K. This is expected as the as-synthesized compound does not contain any accessible channel. But to our surprise at 195 K it adsorbs CO_2 (kinetic diameter, 3.3 Å) gas and at ~1 atm pressure it adsorbs up to 7 wt % of CO_2 (Figure 6).

The calculated Langmuir surface area is 175 m^2/g, a value that is not possible as long as the structure remains rigid. As

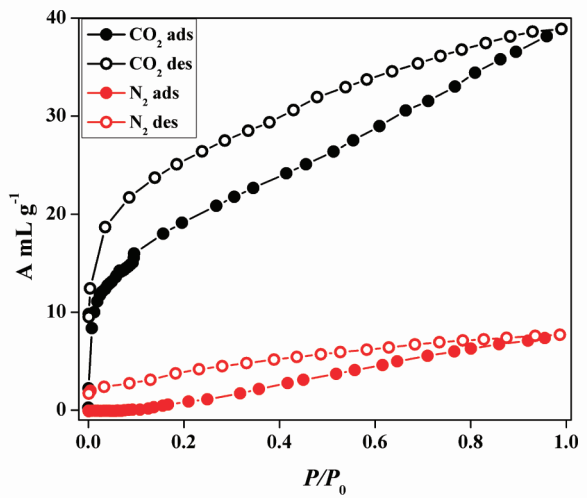

Figure 6. Adsorption–desorption profile for compound **1**. CO_2 at 195 K, N_2 at 77 K.

dx.doi.org/10.1021/ic2027362 | Inorg. Chem. 2012, 51, 4265–4273

from the structure it is evident that the pore size is small (potential guest accessible void volume of 81.7 Å^3 (1.0%) per unit cell volume), and it is decorated with the phenyl groups from the phenylcetate. The phenyl groups which are linked with the flexible $-CH_2$ group through a single bond, would reorient according to the interactions with the incoming guest molecules to make a passage for the accommodation in the pore. In fact, this reorientation allows an effective interaction of the CO_2 molecule (that has a high quadrupole moment of -1.4×10^{-39} C m^2) with the aromatic electron cloud of the phenyl rings. The interaction of the CO_2 molecules with the pore surfaces has been further supported by the hysteretic adsorption behavior with CO_2. Therefore, the flexible pore structure together with the smaller kinetic diameter of CO_2 seem to be the driving forces which finally create an open structure with a small channel along the *b* direction (Figure 7).

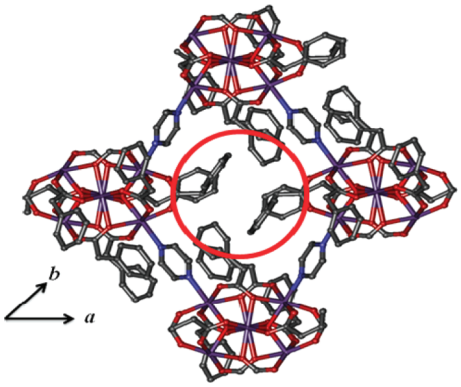

Figure 7. View along the *b* direction of the possible reorientation of the benzyl groups.

Accordingly, we observe a type-I isotherm for CO_2 adsorption. While the absence of a quadrupole moment and the larger kinetic diameter of N_2 are the main reasons that explain the lack of N_2 adsorption and, therefore, the high selectivity toward CO_2,[34] a distinct hysteresis in adsorption−desorption isotherm suggests a stronger interaction of CO_2 with the pore surfaces which is also reflected in a considerably high isosteric heat of adsorption $q_{st,\phi}$ (~ 29 kJ mol^{-1}) as calculated from the Dubinin−Radushkevich (DR) equation.[35]

Magnetic Properties. The thermal variation of the product of the molar magnetic susceptibility per [Mn_6] cluster, times the temperature ($\chi_m T$) of compound **1** shows a room temperature value of about 19.2 emu K mol^{-1}, which is lower than the expected value (23.5 emu K mol^{-1}) for four Mn(II) (S = 5/2) and two Mn(III) (S = 2) isolated ions (Figure 8). When the temperature is lowered, the $\chi_m T$ product shows a progressive decrease down to about 50 K and a more abrupt decrease at lower temperatures to reach a value of about 0.5 emu K mol^{-1} at 2 K. This behavior suggests the presence of predominant antiferromagnetic exchange interactions inside the [Mn_6] cluster which are already operative at high temperatures, as indicated by the low $\chi_m T$ value observed at room temperature. A confirmation of this behavior is provided by the plot of the thermal variation of χ_m that shows a maximum at about 20 K (inset in Figure 8).

Although the structure of this compound shows that the [Mn_6] clusters are connected through pyrazine bridges with four other clusters in a diamond-like 3d arrangement, we can neglect the magnetic coupling through these bridges since the

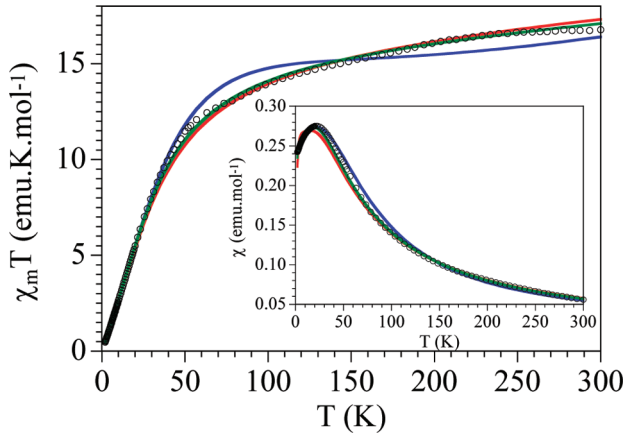

Figure 8. Thermal variation of the $\chi_m T$ product per [Mn_6] cluster for compound **1**. Inset shows the thermal variation of the magnetic susceptibility, χ_m. Blue, red, and green lines are the best fits to the 2JA, 2JB, and 3J models, respectively (see text).

shortest Mn−Mn distance through these pyrazine bridges is about 7.5 Å. Therefore, we can assume that the magnetic properties in this compound correspond to those of the isolated [Mn_6] clusters. A close inspection of these clusters (Figure 9) shows the presence of four different manganese centers (Mn1−Mn4) which are connected in a rectangular array through either double or single oxido bridges plus additional carboxylato bridges connecting all the possible pairs of Mn ions except the central Mn1−Mn2 one (Figure 9).

Although the total number of different magnetic exchange pathways is six (Mn1−Mn2, Mn1−Mn3, Mn1−Mn4, Mn2−Mn3, Mn2−Mn4, and Mn3−Mn4), to fit the magnetic data with a smaller number of parameters, we have assumed in a first approach that all the double oxido plus carboxylato bridges are equivalent (Mn1−Mn2 = Mn1−Mn3 = Mn2−Mn4 = J_1) as well as all the single oxido plus carboxylato ones (Mn1−Mn4 = Mn2−Mn3 = Mn3−Mn4 = J_2). Furthermore, in this simplified model we assume that the central double oxido Mn1−Mn2 bridge is similar to J_1 even if there is no additional carboxylato bridge. (i.e., J_3 = J_1 in the scheme in Figure 9b). Finally, although the two central Mn ions (Mn1 and Mn2) are Mn(III) and the four peripheral Mn ions (two Mn3 and two Mn4) are Mn(II), we assume that both ions have the same g value. This simplified model (*2JA*) is able to reproduce the general shape of the $\chi_m T$ and χ_m plots of compound **1** with the following parameters: g = 2.35(2), J_1 = −66.4 cm^{-1}, and J_2 = −35.8 cm^{-1} ($R = 8.0 \times 10^{-4}$) (blue line in Figure 8, the Hamiltonian is written as $H = -JS_iS_{i+1}$). Albeit, this model does not reproduce satisfactorily the $\chi_m T$ plot at high temperatures and gives a very high g value.

A close inspection at the Mn−O bond lengths in the oxido bridges shows that the double oxido bridge (O1 and O1*) connecting the two central Mn(III) ions (Mn1 and Mn2) presents much shorter Mn−O bond lengths (Mn1−O1 = 1.887(3) and Mn2−O1 = 1.900(3) Å) compared with the other Mn−O bond lengths (all in the range 2.19−2.34 Å). Accordingly, we have assumed that the exchange coupling through this double oxido bridge should be different (most probably stronger) and in a second fit we have included a third exchange coupling (J_3) to reproduce this shorter bridge (Figure 9b). This model with three exchange parameters (*3J*) reproduces very satisfactorily the magnetic data of compound **1** in the whole temperature range with the following

dx.doi.org/10.1021/ic2027362 | Inorg. Chem. 2012, 51, 4265−4273

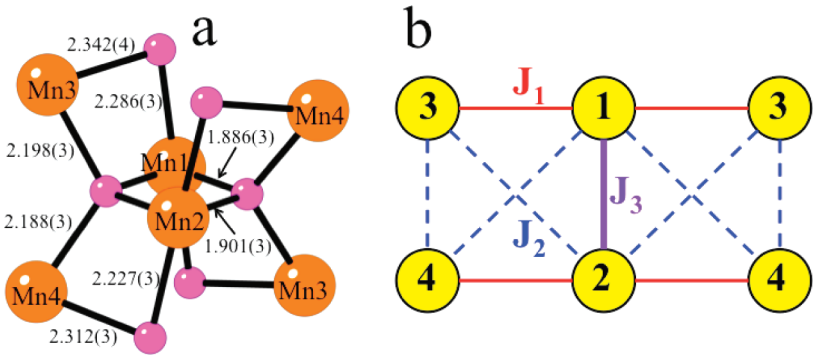

Figure 9. (a) Central $[Mn_6]$ cluster with the Mn−O bond lengths. All the carboxylato bridges connecting the Mn1 and Mn4 with all the other Mn centers are omitted for clarity. (b) Scheme of the magnetic exchange pathway in the $[Mn_6]$ cluster.

parameters: g = 1.983(4), J_1 = −8.6 cm^{-1}, J_2 = −3.9 cm^{-1}, and J_3 = −100.0 cm^{-1} (R = 1.7 × 10^{-4}) (green line in Figure 8). The small deviations observed at low temperature between the experimental and theoretical plots can be easily explained given the simplifications assumed in the model (we have assumed that all the single oxido bridges are equivalent, as well as all the double oxido ones, except the one through O1 and O1*). Finally, to check if the better fit of this last model is simply due to the increase in the number of adjustable parameters, we have fit the magnetic data with a third model that considers that all the coupling constants are equal (J_1) except the one of the central bridge connecting Mn1 with Mn2 (J_3), that is, this model corresponds to the case $J_1 = J_2$ in Figure 9.b) This model (2*JB*) also reproduces very well the magnetic properties of the Mn_6 complex with the following parameters: g = 1.99(1), J_1 = −5.0 cm^{-1} and J_3 = −100.0 cm^{-1}(R = 7 × 10^{-4}) (red line in Figure 8). As expected, this model gives a more realistic g value and reproduces the magnetic data much better that model 2*JA*, confirming the idea that the central Mn1−Mn2 coupling constant is different and stronger than all the other bridges.

The $[Mn_6O_2(PhCH_2COO)_{10}]$ cluster present in compound **1** is quite common: a search in the CCDC database (updated to Nov 2011) shows a total of 31 $[Mn_6O_2(RCOO)_{10}]$ clusters with the same connectivity as the $[Mn_6O_2]$ cluster in compound **1**. By far, the two most common carboxylato ligands found in these clusters are the pivalate (Me_3C-COO^-) anion (with 17 examples)[9a,10a,19d,36] and the benzoate ($PhCOO^-$) anion (with 7 examples).[9a−c,37] The other carboxylate anions used are CH_3COO^-,[19b] $CHCl_2COO^-$,[38] CCl_3COO^-,[21] CBr_3COO^-,[39] $CH_3CH_2COO^-$,[8b] F_4PhCOO^-,[40] and $(NO_2)_2PhCOO^-$,[37b] with one example of each. Compound **1** is, therefore, the first known example of $[Mn_6O_2(RCOO)_{10}]$ cluster with the $PhCH_2COO^-$ anion.

Even if the structure of the $[Mn_6O_2(RCOO)_{10}]$ cluster is quite common, only 17 of the 31 known examples have been magnetically characterized.[8b,9a,10a,19a,20,36c,38,40] All of them show moderate antiferromagnetic exchange couplings although only in two cases have the magnetic properties been modeled.[9b,c] As expected, the exchange coupling constants obtained in the fit of compound **1** are very similar to those obtained in these two similar $[Mn_6O_2(OOCR)_{10}]$ clusters (Table 1). In both clusters the strongest coupling is observed between the central Mn(III) ions whereas the coupling between the peripheral Mn(II) ions is found to be much weaker. Although the models used in these two other $[Mn_6]$ clusters are not exactly the same, the different models used in the present study have evidenced that the most important feature to reproduce the magnetic properties is the presence of a strong magnetic coupling between the central Mn(III) ions, the other exchange pathways being less relevant. This strong coupling between the central Mn(III) ions correlate well with the expected value from magneto-structural correlations and theoretical calculations.[41] Finally, as already pointed out by Hendrickson et al., the exchange between the Mn(II) and the Mn(III) as well as between the Mn(II) atoms of the periphery is expected to be AF and moderate.[9c]

Table 1. Magnetic Exchange Parameters Obtained in Similar $[Mn_6O_2(RCOO)_{10}]$ Clusters

CCDC code	J_1 (cm^{-1})[a,b]	J_2 (cm^{-1})[a,b]	J_3 (cm^{-1})[a,b]	ref.
SAVJEE	−4.8	−1.6	−84.0	9c
RASNOP	−8.3[c]	−4.2[c]	−101.0	9b
1	−8.6[d]	−3.9[d]	−100.0	this work

[a] J_1, J_2, and J_3 correspond to the Mn(II)−Mn(II), Mn(II)−Mn(III), and Mn(III)−Mn(III) exchange coupling, respectively. [b] The Hamiltonian is written as $H = -JS_iS_{i+1}$ in all cases. [c] J_1 corresponds to the single oxido bridge between Mn(II) ions and J_2 to all the remaining exchange coupling (except the central Mn(III)−Mn(III) coupling). [d] J_1 and J_2 correspond to the double and single oxido bridges, respectively.

Finally, the isothermal magnetization at 2 K (Supporting Information, Figure S3) shows a low value of the magnetization and a linear increase with increasing the magnetic field, in agreement with the antiferromagnetic coupling present in this compound. The residual magnetization at 5 T corresponds to the presence of a small amount of paramagnetic impurities due to the presence of crystal defects and vacancies and is well below the expected value (ca. 24 μ_B) for four Mn(II) and two Mn(III) ions with $g \approx 2$.

CONCLUSIONS

Compound **1** is the first $[Mn_6O_2(RCOO)_{10}]$ cluster with phenylacetate as carboxylate ligand and is the first example of a diamond-like structure formed from this kind of $[Mn_6O_2(RCOO)_{10}]$ clusters. This pyrazine bridged porous 3D MOF of mixed valence magnetic $[Mn_6O_2]$ cluster shows selective CO_2 adsorption over N_2 and is also very efficient in catecholase activity. Therefore, compound **1** constitutes a rare example of multifunctionality in a molecule-based material.

ASSOCIATED CONTENT

Supporting Information

IR spectra of complex **1**, C−H···π supramolecular interaction in complex **1**, and isothermal magnetization of compound **1** at 2 K are represented in Figures S1, S2 and S3, respectively. Crystal

dx.doi.org/10.1021/ic2027362 | Inorg. Chem. 2012, 51, 4265−4273

data and structure refinement of complex **1** and bond lengths (Å) and angles (deg) in the metal coordination spheres of the Mn ions in complex **1** are presented in Table-ST1 and Table-ST2, and crystallographic data in CIF format for the structure reported. This material is available free of charge via the Internet at http://pubs.acs.org.

AUTHOR INFORMATION

Corresponding Author

* E-mail: carlos.gomez@uv.es (C.J.G.-G.), ghosh_59@yahoo.com (A.G.).

Notes

The authors declare no competing financial interest.

ACKNOWLEDGMENTS

P.K. is thankful to CSIR, India, for research fellowship [Sanction no. 09/028(0733)/2008-EMR-I]. Crystallography was performed at the DST-FIST, India-funded Single Crystal Diffractometer Facility at the Department of Chemistry, University of Calcutta. We thank the Spanish Ministerio de Ciencia e Innovacion (Projects Consolider-Ingenio in Molecular Nanoscience CSD2007-00010 and CTQ-2011-26507) and the Generalitat Valenciana (Project Prometeo 2009/95). We are thankful to Prof. Michael G. B. Drew, School of Chemistry, The University of Reading, U.K., for helpful discussions on the crystallographic part.

REFERENCES

(1) (a) Qiu, S.; Zhu, G. *Coord. Chem. Rev.* **2009**, *253*, 2891−2911. (b) Decurtins, S.; Pellaux, R.; Antorrena, G.; Palacio, F. *Coord. Chem. Rev.* **1999**, *190*−*192*, 841−854. (c) Chelebaeva, E.; Larionova, J.; Guari, Y.; SaFerreira, R. A.; Carlos, L. D.; Paz, F. A. A.; Trifonov, A.; Guerin, C. *Inorg. Chem.* **2008**, *47*, 775−777. (d) Kitagawa, S.; Kitaura, R.; Norc, S. *Angew. Chem., Int. Ed.* **2004**, *43*, 2334−2375. (e) Forster, P. M.; Eckert, J.; Heiken, B. D.; Parise, J. B.; Yoon, J. W.; Jhung, S. H.; Chang, J.-S.; Cheetham, A. K. *J. Am. Chem. Soc.* **2006**, *128*, 16846−16850. (f) Kar, P.; Guha, P. M.; Drew, M. G. B.; Ishida, T.; Ghosh, A. *Eur. J. Inorg. Chem.* **2011**, 2075−2085. (g) Kar, P.; Biswas, R.; Drew, M. G. B.; Ida, Y.; Ishida, T.; Ghosh, A. *Dalton Trans.* **2011**, *40*, 3295−3304.

(2) (a) Qiao, X.-F.; Yan, B. *Inorg. Chem.* **2009**, *48*, 4714−4723. (b) Gu, Z.-G.; Zhou, X.-H.; Jin, Y.-B.; Xiong, R.-G.; Zuo, J.-L.; You, X.-Z. *Inorg. Chem.* **2007**, *46*, 5462−5464. (c) Cheetham, A. K.; Rao, C. N. R. *Science.* **2007**, *318*, 58−59. (d) Férey, G.; Millange, F.; Morcrette, M.; Serre, C.; Doublet, M.-L.; Greneche, J.-M.; Tarascon, J.-M. *Angew. Chem., Int. Ed.* **2007**, *46*, 3259−3263. (e) Tanaka, D.; Kitagawa, S. *MRS Bull.* **2007**, *32*, 540−543.

(3) (a) Li, H.; Eddaoudi, M.; O'Keeffe, M.; Yaghi, O. M. *Nature.* **1999**, *402*, 276−279. (b) Tao, J.; Yin, X.; Wei, Z.-B.; Huang, R.-B.; Zheng, L.-S. *Eur. J. Inorg. Chem.* **2004**, 125−133. (c) Zhang, J. J.; Lachgar, A. *J. Am. Chem. Soc.* **2007**, *129*, 250−251. (d) Zhang, X. M.; Fang, R. Q.; Wu, H. S. *J. Am. Chem. Soc.* **2005**, *127*, 7670−7671. (e) Ma, C.-B.; Chen, C.-N.; Liu, Q.-T.; Liao, D.-Z.; Li, L.-C. *Eur. J. Inorg. Chem.* **2008**, 1865−1870.

(4) (a) Lampropoulos, C.; Redler, G.; Data, S.; Abboud, K. A.; Hill, S.; Christou, G. *Inorg. Chem.* **2010**, *49*, 1325−1336. (b) Miyasaka, H.; Saitoh, A.; Abe, S. *Coord. Chem. Rev.* **2007**, *251*, 2622−2664. (c) Costa, J. S.; Barrios, L. A.; Craig, G. A.; Teat, S. J.; Luis, F.; Roubeau, O.; Evangelisti, M.; Camón, A.; Aromí, G. *Chem. Commun.* **2012**, *48*, 1413−1415. (d) Mondal, K. C.; Song, Y.; Mukherjee, P. S. *Inorg. Chem.* **2007**, *46*, 9736−9742. (e) Mondal, K. C.; Drew, M. G. B.; Mukherjee, P. S. *Inorg. Chem.* **2007**, *46*, 5625−5629.

(5) (a) Ferreira, K. N.; Iverson, T. M.; Maghlaoui, K.; Barber, J.; Iwata, S. *Science.* **2004**, *303*, 1831−1838. (b) Rutherford, A. W.; Boussac, A. *Science.* **2004**, *303*, 1782−1784. (c) Mukhopadhyay, S.; Mandal, S. K.; Bhaduri, S.; Armstrong, W. H. *Chem. Rev.* **2004**, *104*, 3981−4026. (d) Rappaport, F.; Diner, B. A. *Coord. Chem. Rev.* **2008**, *252*, 259−272. (e) Carboni, M.; Latour, J.-M. *Coord. Chem. Rev.* **2011**, *255*, 186−202.

(6) (a) Venkataramanan, N. S.; Kuppuraj, G.; Rajagopal, S. *Coord. Chem. Rev.* **2005**, *249*, 1249−1268. (b) Katsuki, T. *Coord. Chem. Rev.* **1995**, *140*, 189−214.

(7) (a) Feng, P. L.; Hendrickson, D. N. *Inorg. Chem.* **2010**, *49*, 6393−6395. (b) Moushi, E. E.; Stamatatos, T. C.; Wernsdorfer, W.; Nastopoulos, V.; Christou, G.; Tasiopoulos, A. J. *Inorg. Chem.* **2009**, *48*, 5049−5051. (c) Taguchi, T.; Wernsdorfer, W.; Abboud, K. A.; Christou, G. *Inorg. Chem.* **2010**, *49*, 199−208.

(8) (a) Nakata, K.; Miyasaka, H.; Sugimoto, K.; Ishii, T.; Sugiura, K.; Yamashita, M. *Chem. Lett.* **2002**, 658−660. (b) Ma, C.-B.; Hu, M.-Q.; Chen, H.; Chen, C.-N.; Liu, Q.-T. *Eur. J. Inorg. Chem.* **2008**, 5274−5280.

(9) (a) Fursova, E.; Ovcharenko, V.; Nosova, K.; Romanenko, G.; Ikorskii, V. *Polyhedron* **2005**, *24*, 2084−2093. (b) Gavrilenko, K. S.; Punin, S. V.; Cador, O.; Golhen, S.; Ouahab, L.; Pavlishchuk, V. V. *Inorg. Chem.* **2005**, *44*, 5903−5910. (c) Schake, A. R.; Vincent, J. B.; Li, Q.; Boyd, P. D. W.; Folting, K.; Huffman, J. C.; Hendrickson, D. N.; Christou, G. *Inorg. Chem.* **1989**, *28*, 1915−1923.

(10) (a) Ovcharenko, V.; Fursova, E.; Romanenko, G.; Ikorskii, V. *Inorg. Chem.* **2004**, *43*, 3332−3334. (b) Malaestean, I. L.; Kravtsov, V. Ch.; Speldrich, M.; Dulcevscaia, G.; Simonov, Y. A.; Lipkowski, J.; Ellern, A.; Baca, S. G.; Kogerler, P. *Inorg. Chem.* **2010**, *49*, 7764−7772.

(11) (a) Lieb, D.; Zahl, A.; Shubina, T. E.; Ivanovic-Burmazovic, I. *J. Am. Chem. Soc.* **2010**, *132*, 7282−7284. (b) Kani, I.; Darak, C.; Şahin, O.; Büyükgüngör, O. *Polyhedron* **2008**, *27*, 1238−1247. (c) Maayan, G.; Christou, G. *Inorg. Chem.* **2011**, *50* (15), 7015−7021. (d) Mukherjee, P.; Kar, P.; Ianelli, S.; Ghosh, A. *Inorg. Chim. Acta* **2011**, *365*, 318−324.

(12) Bain, G. A.; Berry, J. F. *J. Chem. Educ.* **2008**, *85*, 532−536.

(13) *SAINT*, version 6.02; *SADABS*, version 2.03; Bruker AXS, Inc.: Madison, WI, 2002.

(14) Sheldrick, G. M. *SHELXS 97, Program for Structure Solution*; University of Göttingen: Göttingen, Germany, 1997.

(15) Sheldrick, G. M. *SHELXL 97, Program for Crystal Structure Refinement*; University of Göttingen: Göttingen, Germany, 1997.

(16) *PLATON, Molecular Geometry Program*; Spek, A. L. *J. Appl. Crystallogr.* **2003**, *36*, 7−13.

(17) Farrugia, L. J. *J. Appl. Crystallogr.* **1997**, *30*, 565.

(18) Farrugia, L. J. *J. Appl. Crystallogr.* **1999**, *32*, 837−838.

(19) (a) Stamatatos, T. C.; Foguet-Albiol, D.; Perlepes, S. P.; Raptopoulou, C. P.; Terzis, A.; Patrickios, C. S.; Christou, G.; Tasiopoulos, A. J. *Polyhedron* **2006**, *25*, 1737−1746. (b) Karsten, P.; Strahle, J. *Acta Crystallogr.* **1998**, *C54*, 1403−1406. (c) Sarı, M.; Poyraz, M.; Buyukgungor, O. *J. Chem. Crystallogr.* **2009**, *39*, 549−552. (d) Kiskin, M. A.; Fomina, I. G.; Aleksandrov, G. G.; Sidorov, A. A.; Novotortsev, V. M.; Rakitin, Y. V.; Dobrokhotova, Z. V.; Ikorskii, V. N.; Shvedenkov, Y. G.; Eremenko, I. L.; Moiseev, I. I. *Inorg. Chem. Commun.* **2005**, *8*, 89−93.

(20) Kim, J.; Cho, H. *Inorg. Chem. Commun.* **2004**, *7*, 122−124.

(21) (a) Blake, A. J.; Champness, N. R.; Khlobystov, A. N.; Lemenovskii, D. A.; Li, W.-S.; Schroder, M. *Chem. Commun.* **1997**, 1339−1340. (b) MacGillivray, L. R.; Subramanian, S.; Zoworotko, M. J. *J. Chem. Soc., Chem. Commun.* **1994**, 1325−1326. (c) Hoskins, B. F.; Robson, R. *J. Am. Chem. Soc.* **1990**, *112*, 1546−1554.

(22) (a) Liang, K.; Zheng, H.; Song, Y.; Lappert, M. F.; Li, Y.; Xin, X.; Huang, Z.; Chen, J.; Lu, S. *Angew. Chem., Int. Ed.* **2004**, *43*, 5776−5779. (b) Wang, X.-S.; Zhao, H.; Qu, H. Z.-R.; Ye, Q.; Zhang, J.; Xiong, R.-G.; You, X.-Z.; Fun, H.-K. *Inorg. Chem.* **2003**, *42*, 5786−5788.

(23) (a) Konar, S.; Zangrando, E.; Drew, M. G. B.; Ribas, J.; Chaudhuri, N. R. *Dalton Trans.* **2004**, 260−266. (b) Evans, O. R.; Lin, W. *Acc. Chem. Res.* **2002**, *35*, 511−522. (c) Lin, W.; Ma, L.; Evans, O. R. *Chem. Commun.* **2000**, 2263−2264. (d) Laskoski, M. C.; LaDuca, R. L. Jr.; Rarig, R. S. Jr.; Zubieta, J. *J. Chem. Soc., Dalton Trans.* **1999**, 3467−3472.

(24) Mukherjee, J.; Mukherjee, R. *Inorg. Chim. Acta* **2002**, *337*, 429–438.
(25) Banu, K. S.; Chattopadhyay, T.; Banerjee, A.; Mukherjee, M.; Bhattacharya, S.; Patra, G. K.; Zangrando, E.; Das, D. *Dalton Trans.* **2009**, 8755–8764.
(26) (a) Koval, I. A.; Gamez, P.; Belle, C.; Selmeczi, K.; Reedijk, J. *Chem. Soc. Rev.* **2006**, *35*, 814–840. (b) Bhardwaj, V. K.; Aliaga-Alcalde, N.; Corbella, M.; Hundal, G. *Inorg. Chim. Acta* **2010**, *363*, 97–106.
(27) (a) Mukherjee, S.; Weyhermuller, T.; Bothe, E.; Wieghardt, K.; Chaudhuri, P. *Dalton Trans.* **2004**, 3842–3853. (b) Majumder, A.; Goswami, S.; Batten, S. R.; Fallah, M. S. E.; Ribas, J.; Mitra, S. *Inorg. Chim. Acta* **2006**, *359*, 2375–2382. (c) Jones, S. E.; Chin, D.-H.; Sawyer, D. T. *Inorg. Chem.* **1981**, *20*, 4257–4262.
(28) (a) Guha, A.; Banu, K. S.; Banerjee, A.; Ghosh, T.; Bhattacharya, S.; Zangrando, E.; Das, D. *J. Mol. Catal. A: Chem.* **2011**, *338*, 51–57. (b) Kaizer, J.; Barath, G.; Csonka, R.; Speier, G.; Korecz, L.; Rockenbauer, A.; Parkanyi, L. *J. Inorg. Biochem.* **2008**, *102*, 773–780. (c) Kloskowski, M.; Krebs, B. *Z. Anorg. Allg. Chem.* **2006**, *632*, 771–778.
(29) Triller, M. U.; Pursche, D.; Hsieh, W.-Y.; Pecoraro, V. L.; Rompel, A.; Krebs, B. *Inorg. Chem.* **2003**, *42*, 6274–6283.
(30) (a) Banerjee, A.; Sarkar, S.; Chopra, D.; Colacio, E.; Rajak, K. K. *Inorg. Chem.* **2008**, *47*, 4023–4031. (b) Banerjee, A.; Singh, R.; Colacio, E.; Rajak, K. K. *Eur. J. Inorg. Chem.* **2009**, 277–284.
(31) Sreenivasulu, B.; Vetrichelvan, M.; Zhao, F.; Gao, S.; Vittal, J. J. *Eur. J. Inorg. Chem.* **2005**, 4635–4645.
(32) (a) Xu, R.; Pang, W.; Yu, J.; Huo, Q.; Chen, J. *Chemistry of Zeolites and Related Porous Materials: Synthesis and Structure*; John Wiley & Sons (Asia) Pet Ltd.: Singapore, 2007. (b) Yang, R. T. *Gas Separation by Adsorption Progress*; Butterworth: Boston, 1987. (c) Rouquerol, F.; Rouquerol, I.; Sing, K. *Adsorption by Powders and Porous Solids-Principles Methodology and Applications*; Academic Press: London, U.K., 1999.
(33) Webster, C. E.; Drago, R. S.; Zerner, M. C. *J. Am. Chem. Soc.* **1998**, *120*, 5509–5516.
(34) (a) Kanoo, P.; Haldar, R.; Cyrac, S. T.; Maji, T. K. *Chem. Commun.* **2011**, *47*, 11038–11040. (b) Hazra, A.; Kanoo, P.; Maji, T. K. *Chem. Commun.* **2011**, *47*, 538–540. (c) Kanoo, P.; Sambhu, R.; Maji, T. K. *Inorg. Chem.* **2011**, *50*, 400–402.
(35) Dubinin, M. M. *Chem. Rev.* **1960**, *60*, 235–241.
(36) (a) Gerbier, P.; Ruiz-Molina, D.; Gómez, J.; Wurst, K.; Veciana, J. *Polyhedron.* **2003**, *22*, 1951–1955. (b) Kiskin, M. A.; Sidorov, A. A.; Fomina, I. G.; Rusinov, G. L.; Ishmetova, R. I.; Aleksandrov, G. G.; Shvedenkov, Y. G.; Dobrokhotova, Z. V.; Novotortsev, V. M.; Chupakhin, O. N.; Eremenko, I. L.; Moiseev, I. I. *Inorg. Chem. Commun.* **2005**, *8*, 524–528. (c) Baikie, A. R. E.; Howes, A. J.; Hursthouse, M. B.; Quick, A. B.; Thornton, P. *J. Chem. Soc., Chem. Commun.* **1986**, 1587–1587. (d) Murrie, M.; Parsons, S.; Winpenny, R. E. P. *J. Chem. Soc., Dalton Trans.* **1998**, 1423–1424. (e) Köhler, K.; Roesky, H. W.; Noltemeyer, M.; Schmidt, H.; Freire-Erdbrügger, C.; Sheldrick, G. M. *Chem. Ber.* **1993**, *126*, 921–926.
(37) (a) Blackman, A. G.; Huffman, J. C.; Lobkovsky, E. B.; Christou, G. *Polyhedron.* **1992**, *11*, 251–255. (b) Halcrow, M. A.; Streib, W. E.; Folting, K.; Christou, G. *Acta Crystallogr., Sect. C* **1995**, *51*, 1263–1267.
(38) Kushch, L. A.; Shilov, G. V.; Morgunov, R. B.; Yagubskii, E. B. *Mendeleev Commun.* **2009**, *19*, 170–171.
(39) Gomez-Segura, J.; Lhotel, E.; Paulsen, C.; Luneau, D.; Wurst, K.; Veciana, J.; Ruiz-Molina, D.; Gerbier, P. *New J. Chem.* **2005**, *29*, 499–503.
(40) Nakata, K.; Miyasaka, H.; Ishii, T.; Yamashita, M.; Awaga, K. *Mol. Cryst. Liq. Cryst.* **2002**, *379*, 211–216.
(41) Ruiz, E.; Alvarez, S. *Chem. Commun.* **1998**, 2767–2768.